ACS Photonics

pubs.acs.org/journal/apchd5

Article

Transformation Optics Description of Direct and Cascaded Third-Harmonic Generation

Fan Yang* and Cristian Ciracì

Cite This: https://doi.org/10.1021/acsphotonics.3c00343

Read Online

ACCESS | Metrics & More | Article Recommendations | Supporting Information

ABSTRACT: We analytically study the direct and cascaded third-harmonic generation from a nanowire dimer system with a transformation optics approach. The near-field, emission pattern, spectrum, and size dependence of the nanowire dimer are systematically explored. The calculation reveals that the direct and cascaded third-harmonic generation possess different mode excitations and size dependence for a plasmonic structure made up of centrosymmetric media. We point out that these discrepancies can be utilized as a fingerprint to clarify the nonlinear origin of a measured third-harmonic signal. In addition, a broadband continuous multiresonant state appears when the nanostructure becomes more singular, strongly improving the upconversion efficiency.

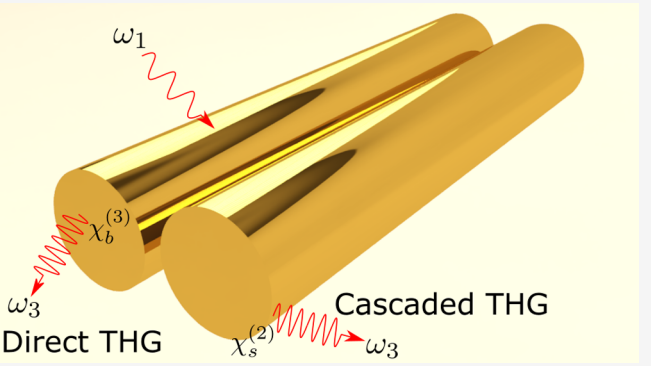

KEYWORDS: *transformation optics, third-harmonic generation, second-harmonic generation, sum-frequency generation, direct and cascaded process, nonlinear surface susceptibility*

Downloaded via NANJING UNIV on August 7, 2023 at 07:15:32 (UTC).
See https://pubs.acs.org/sharingguidelines for options on how to legitimately share published articles.

1. INTRODUCTION

Nonlinear optical effects play an indispensable role in the field of nanophotonics. The introduction of nonlinearity leads to various interesting optical phenomena that linear response cannot offer.[1] For instance, the second or third-harmonic generation (THG) enables frequency upconversion by combining multiple photons into a single photon with a higher frequency. There are two main optical processes for a THG. For one process, three photons with identical energy $\hbar\omega_1$ directly combine and generate a single photon with energy $\hbar\omega_3 = 3\hbar\omega_1$, see Figure 1a. This straightforward process is termed direct THG. On the other hand, in Figure 1b, a photon with energy $\hbar\omega_2 = 2\hbar\omega_1$ is first generated by the interaction of two photons with identical energy $\hbar\omega_1$ through the second-harmonic generation (SHG) process. The generated $\hbar\omega_2$ photon then interacts with a $\hbar\omega_1$ photon through a sum-frequency generation (SFG) process to emit a $\hbar\omega_3$ photon. This two-step second-order nonlinear process is defined as cascaded THG.[2]

Both the direct and cascaded processes generally exist in nonlinear optical responses. However, the most commonly used plasmonic materials, such as gold and silver, are centrosymmetric. In these material systems, second-order nonlinear processes in bulk are forbidden,[1,2] such that the nonlinear optical response can be validly modeled with a nonlinear surface susceptibility $\chi_s^{(2)}$.[3] However, the third-order nonlinear process occurs mainly in bulk for both centrosymmetric and noncentrosymmetric media. Therefore, this nonlinear response can be described with a bulk $\chi_b^{(3)}$. (Note that there might also be third-order surface contributions. Here, however, we neglect them for simplicity.) Given their different physical origins of nonlinearity, many previous works have attempted to characterize these two different nonlinear processes. From the theoretical or numerical point of view, the hydrodynamic model for the free electron dynamics has been applied in modeling these two different nonlinear optical responses.[4] Experimentally, Celebrano et al. have shown that it is possible to distinguish direct from cascaded THG processes by measuring the emission pattern of third-harmonic signals from noncentrosymmetric gold nanoantennas.[5,6]

In this paper, a transformation optics approach[7] is for the first time applied in the characterization of direct and cascaded THG from a nanowire dimer. As a typical prototype, the dimer nanostructure has been extensively employed to investigate various optical effects, such as field localization,[8] surface-enhanced Raman scattering,[9] nonlocal effect,[10,11] electron spill-out and tunneling,[12−15] strong coupling,[16] and van der Waals interactions.[17] Moreover, in the aspect of nonlinearity, the introduction of transformation optics allows an analytical

Received: March 13, 2023

© XXXX American Chemical Society

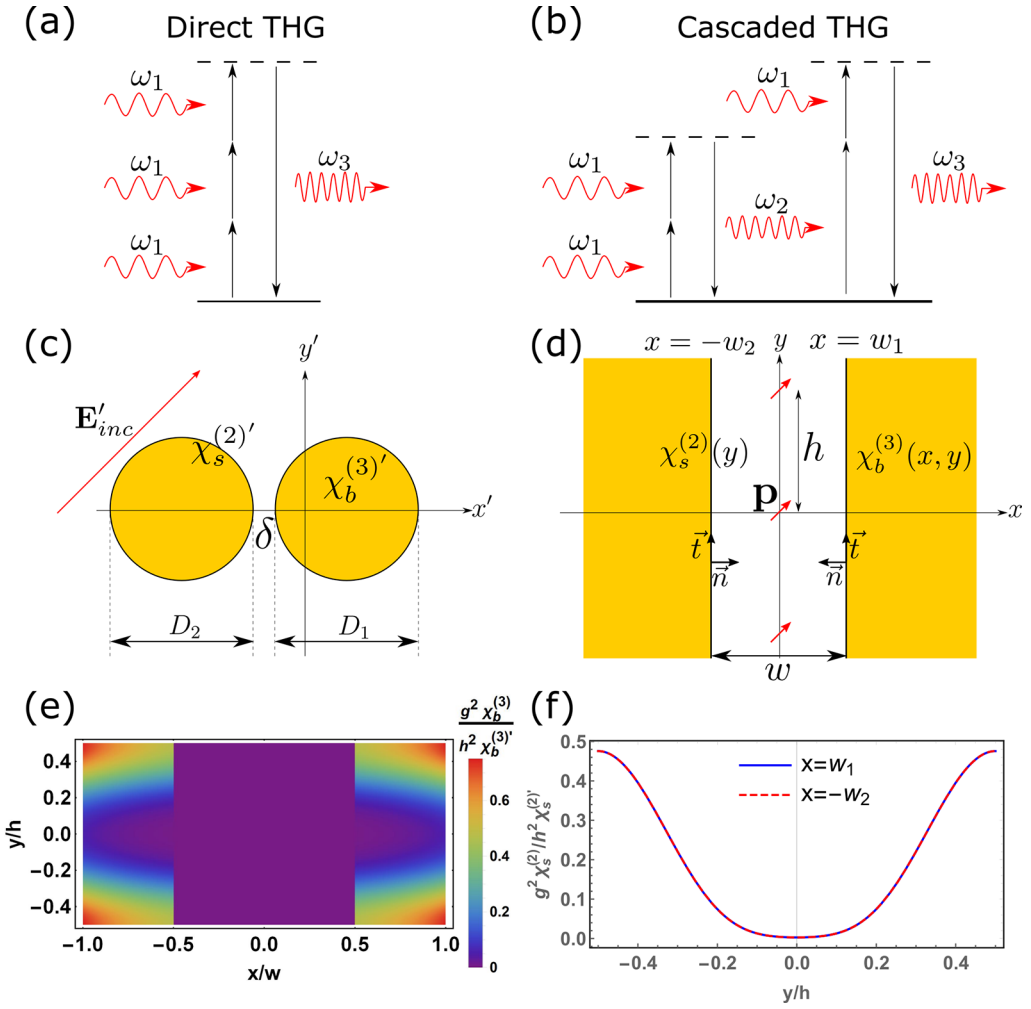

Figure 1. Schematic for THG from a nanowire dimer. (a) Energy level diagram for direct THG process, where the solid and dashed lines represent the atomic ground state and virtual energy level, respectively; (b) The energy level for the cascaded THG process, which consists of an SHG process and a subsequent SFG process; (c) The nanowire dimer system. The nanowire dimer system is parametrized by $D_{1,2}$ (the nanowire diameter) and δ (the gap between two nanowires); (d) The mapped metal−insulator−metal (MIM) cavity structure. The cavity width is w, and the transformation of eq 1 converts a uniform electric field in the dimer frame into a dipole array (red arrows) with period h in the MIM frame. The directions of $\perp$ and $\parallel$ at the metal surface are defined as $\vec{n}$ and $\vec{t}$, respectively; (e, f) The profile of $\chi_b^{(3)}(x, y)$ (panel (e)) and $\chi_s^{(2)}(y)$ (panel (f)) in the MIM frame for a nanowire dimer parametrized with $D_1 = D_2 = 6$ nm and $\delta = 1$ nm.

solution to the nonlinear optical response.[18−20] With this powerful tool, we analytically examined both direct and cascaded THG from a nanowire dimer and found that these two processes possess some similarities but also a few thrilling discrepancies in the spectrum and size dependence.

2. SCHEMATIC

Let us consider a plasmonic nanowire dimer as depicted in Figure 1c. The plasmonic material (yellow region) follows a Drude model permittivity, $\varepsilon = 1 - \omega_p^2/(\omega^2 + i\omega\gamma)$, with $\gamma = 0.01\omega_p$. The plasmonic frequency is $\omega_p = \sqrt{\frac{e^2 n_0}{\varepsilon_0 m_e}}$,[21,22] where the electron density $n_0 = 5.97 \times 10^{28}$ m^{-3}, a typical value for the gold's electron density. We stress that a nanowire dimer is just a prototype demonstrating our theoretical framework. Other structures, such as kissing nanowires,[23] a particle on the mirror,[24] and singular metasurfaces,[25,26] can be analyzed similarly. The space where the dimer resides is defined as the physical space, where the complex coordinate is $z' = x' + iy'$. Under the excitation of the TM incident light, $\mathbf{E}'_{\text{inc}}$ (with a peak intensity of 55 MW/cm^2) polarized in the $x'-y'$ plane, the plasmonic modes of the nanowire dimer are excited, which localizes and enhances the electric field. The excited field behaves as a pump that gives rise to a nonlinear polarization, generating high-harmonic fields. To further obtain the analytical solution of the nonlinear response of the dimer system, the nanowire dimer is mapped into a metal−insulator−metal (MIM) heterostructure with a cavity width w in Figure 1d by using the following transformation[8]

$$z' = \frac{g}{e^{2\pi/hz^*} - 1} \tag{1}$$

where g is an arbitrary constant, $z' = x' + iy'$ and $z = x + iy$ represent the complex coordinates of the dimer frame and MIM frame, respectively. The essence of this transformation is that the complex dimer geometry is converted into a much simpler MIM structure, where the analytical calculation is implemented. The mode excitation considered in our study is a plane wave in the dimer frame, which is converted into a dipole array with dipole moment $\mathbf{p} = \varepsilon_0 gh\mathbf{E}'_{\text{inc}}$ in the MIM frame. For

https://doi.org/10.1021/acsphotonics.3c00343
ACS Photonics XXXX, XXX, XXX−XXX

simplicity, we utilize the undepleted-pump approximation, i.e., the second and third-harmonic field does not affect the optical response at ω_1. Throughout this paper, the polarization, electric field, and nonlinear susceptibility with/without primes stand for the physical quantities in the dimer/MIM frame.

The coordinate-independent nonlinear susceptibilities $\chi_s^{(2)'}$ and $\chi_b^{(3)'}$ in the dimer frame (physical space), when mapping into the MIM frame (virtual space), obtain a dependence on coordinates. The explicit expressions for their mapping read

$$\chi_b^{(3)}(x, y) = \left|\frac{dz}{dz'}\right|^2 \chi_b^{(3)'} = \frac{h^2}{4\pi^2 g^2}(e^{Gx} + e^{-Gx} - e^{iGy} - e^{-iGy})^2 \chi_b^{(3)'} \tag{2}$$

and

$$\chi_s^{(2)}(y) = \left|\frac{dz}{dz'}\right|^2 \chi_s^{(2)'}\Big|_{x=w_1(-w_2)} = \frac{h^2}{4\pi^2 g^2}(e^{Gx} + e^{-Gx} - e^{iGy} - e^{-iGy})^2 \chi_s^{(2)'}\Big|_{x=w_1(-w_2)} \tag{3}$$

where $G = 2\pi/h$ (see Supporting Information). It is interesting that $\chi_s^{(2)}$ and $\chi_b^{(3)}$ have the same mapping rule, except that $\chi_s^{(2)}$ is only evaluated on the metal surface $x = w_1$ or $x = -w_2$ in the MIM frame. The coordinate dependences of these two nonlinear susceptibilities are illustrated in Figure 1e,f. According to the transformation in eq 1, the gap region in the dimer frame is mapped into $y = \pm h/2$ in the MIM frame, where the nonlinear susceptibility is higher than the other region.

For the direct THG, we assume that the nonlinear response originates in the bulk. The direct nonlinear process then leads to a bulk nonlinear polarization at the third-harmonic frequency ω_3 in Figure 1d, which reads as[1]

$$\mathbf{P}^{\mathrm{NL}} = \varepsilon_0 \chi_b^{(3)}(\mathbf{E}_1 \cdot \mathbf{E}_1)\mathbf{E}_1 \tag{4}$$

where the third-order nonlinear susceptibility $\chi_b^{(3)}$ can be evaluated by substituting $\chi_b^{(3)'} = 10^{-18}$ m^2/V^2 (a typical value for gold[27]) into eq 2. Note that the direct third-order nonlinear process also contributes to Kerr nonlinearity,[1] which does not affect the direct THG with the undepleted-pump approximation.

On the other hand, the cascaded THG consists of two second-order nonlinear processes. The quantitative description requires $\chi_s^{(2)'}(\omega_2 = \omega_1 + \omega_1)$ for the first SHG and $\chi_s^{(2)'}(\omega_3 = \omega_2 + \omega_1)$ for the subsequent SFG process. We derive the expression for these nonlinear surface susceptibilities from hydrodynamic theory,[4,28,29] which reads

$$\chi_{\perp\perp_1\perp_1}^{(2)'} = \frac{\varepsilon_0}{4en_0}\frac{3\omega_1 + i\gamma}{2\omega_1 + i\gamma}(\varepsilon(\omega_1) - 1)^2$$
$$\chi_{\parallel\perp_1\parallel_1}^{(2)'} = \frac{\varepsilon_0}{2en_0}(\varepsilon(\omega_1) - 1)^2 \tag{5}$$

for SHG and

$$\chi_{\perp\perp_1\perp_2}^{(2)'} = \frac{\varepsilon_0}{2en_0}\frac{\omega_3^2 + i\gamma\omega_3 + 2\omega_1\omega_2}{\omega_3^2 + i\gamma\omega_3}(\varepsilon(\omega_1) - 1)(\varepsilon(\omega_2) - 1)$$
$$\chi_{\parallel\perp_1\parallel_2}^{(2)'} = \frac{\varepsilon_0}{en_0}\frac{\omega_2}{\omega_3}(\varepsilon(\omega_1) - 1)(\varepsilon(\omega_2) - 1)$$
$$\chi_{\parallel\perp_2\parallel_1}^{(2)'} = \frac{\varepsilon_0}{en_0}\frac{\omega_1}{\omega_3}(\varepsilon(\omega_1) - 1)(\varepsilon(\omega_2) - 1) \tag{6}$$

for SFG, where $\varepsilon(\omega_1)$ and $\varepsilon(\omega_2)$ represent the nanowire's permittivity ε evaluated at pump frequency ω_1 and second-harmonic frequency ω_2, respectively. $\perp$ and $\parallel$ stand for the normal and parallel directions at the metal surface. The derivation of these nonlinear surface susceptibilities is detailed in the Supporting Information. With the nonlinear surface susceptibilities in eqs 5 and 6, the induced nonlinear surface polarization in the MIM frame can be evaluated as

$$P_\perp^s(\omega_2 = \omega_1 + \omega_1) = \varepsilon_0 \chi_{\perp\perp_1\perp_1}^{(2)} E_{1\perp} E_{1\perp}$$
$$P_\parallel^s(\omega_2 = \omega_1 + \omega_1) = \varepsilon_0 \chi_{\parallel\perp_1\parallel_1}^{(2)} E_{1\perp} E_{1\parallel}$$
$$P_\perp^s(\omega_3 = \omega_1 + \omega_2) = \varepsilon_0 \chi_{\perp\perp_1\perp_2}^{(2)} E_{1\perp} E_{2\perp}$$
$$P_\parallel^s(\omega_3 = \omega_1 + \omega_2) = \varepsilon_0 \chi_{\parallel\perp_1\parallel_2}^{(2)} E_{1\perp} E_{2\parallel} + \varepsilon_0 \chi_{\parallel\perp_2\parallel_1}^{(2)} E_{2\perp} E_{1\parallel} \tag{7}$$

where the unprimed nonlinear surface susceptibilities are obtained by eq 3, and the electric field in the above expressions is evaluated at the point immediately inside the metal surface of MIM structure.

3. FIELD PROFILE

To calculate the THG, we first calculate the electric field at pump frequency ω_1, shown in Figure 2a. The detailed calculation of the linear optical response of a nanowire dimer has been given in the previous works,[8] and the readers can refer to the Supporting Information for more details. Since the conformal mapping conserves the spectrum for the subwavelength nanostructure,[7] the nanowire dimer and its parent structure (MIM geometry) in the quasistatic limit both support two kinds of modes with opposite symmetry,[30] a_x (symmetric for E_x' concerning the dimer axis) and a_y (antisymmetric for E_x' for the dimer axis). Here the subscript of a_x (a_y) means the mode is excited by the electric field's x (y) component. In the loss spectrum, the a_x (a_y) mode resides below (above) the surface plasmon frequency $\omega_{sp} = \omega_p/\sqrt{2}$. The nanowire dimer considered in this paper is subwavelength, making the dipole radiation dominant and thus exhibiting a "figure eight" emission pattern in Figure 2a. For a_x (a_y) mode, the even function of E_x' (E_y') contributes to a nonzero total dipole moment in the x' (y') direction.

Obtaining the pump electric field $\mathbf{E}_1$, we then calculate the nonlinear optical response at second-harmonic frequency ω_2 following our previous theoretical framework. The two components of the nonlinear surface polarization are associated with two surface currents, written as[20,31,32]

https://doi.org/10.1021/acsphotonics.3c00343
ACS Photonics XXXX, XXX, XXX−XXX

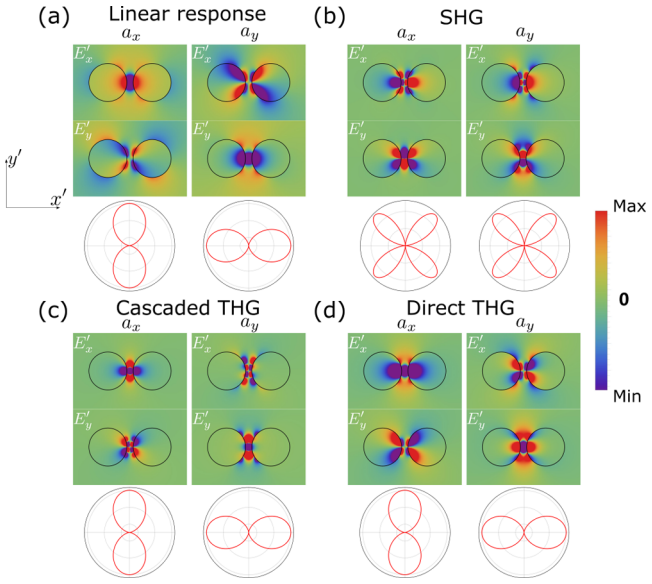

Figure 2. Near field and emission pattern of nanowire dimer ($D_1 = D_2$ = 6 nm and δ = 1 nm) under a pump field excitation for a a_x mode at $\omega_1 = 0.58\omega_p$ and a a_y mode at $\omega_1 = 0.81\omega_p$. (a) Linear optical response at pump frequency ω_1; (b) Second-harmonic response at ω_2; (c) Third-harmonic response at ω_3 for cascaded THG; (d) Third-harmonic response at ω_3 for direct THG.

$$J_m = \frac{1}{\varepsilon_b}\mathbf{n} \times \nabla_{\parallel} P^s_{\perp}$$
$$J_e = \frac{\partial P^s_{\parallel}}{\partial t} \tag{8}$$

where $\nabla_{\parallel}$ stands for the derivative along the parallel direction and ε_b is the background permittivity that equals $\varepsilon_0\varepsilon(\omega_2)$. According to classical electrodynamics, the second-harmonic field excited by the above two currents is derived by matching the tangential electric and magnetic fields at the two metal interfaces $x = w_1$ and $x = -w_2$ in the MIM frame. Note that the electric and magnetic surface currents make the tangential fields discontinuous. Following the rule of transformation optics, the electric field at ω_2 in the MIM frame is then mapped into the dimer frame. The second-harmonic field excited by the pump field of a_x and a_y modes in the dimer frame is shown in Figure 2b. A simple symmetry analysis concludes that both a_x and a_y modes induced SHG gives rise to a zero net dipole moment, making the radiation pattern dominated by the quadrupole, i.e., a petal-like emission pattern.

With the electric field at the pump and second-harmonic frequencies, it is straightforward to calculate the nonlinear polarization $P^s_{\perp,\parallel}(\omega_3 = \omega_1 + \omega_2)$. Similar to the calculation of the SHG process, these nonlinear surface polarizations are linked with an electric and a magnetic surface current with eq 8, except that $\varepsilon_b = \varepsilon_0\varepsilon(\omega_3)$. The detailed derivation can be found in Supporting Information. Figure 2c presents the field profile by the SFG process, i.e., the final cascaded THG. For a_x (a_y) mode, the symmetry for E'_x (E'_y) is even, thereby giving a net dipole moment in x' (y')-direction.

Next, we turn to the direct THG process. The pump field in Figure 2a gives rise to a bulk polarization inside the metal region by eq 4. To figure out the electric field generated by this bulk nonlinear polarization in the MIM frame, we expand the nonlinear polarization in terms of both $e^{ik_{xm}y}$ and $e^{ik_{yn}y}$, which reads

$$P_x^{\mathrm{NL}} = \sum_n \sum_m P_x^{n,m} e^{ik_{xm}x} e^{ik_{yn}y} = \sum_n \sum_m P_x^{n,m} e^{mGx} e^{inGy}$$
$$P_y^{\mathrm{NL}} = \sum_n \sum_m P_y^{n,m} e^{ik_{xm}x} e^{ik_{yn}y} = \sum_n \sum_m P_y^{n,m} e^{mGx} e^{inGy} \tag{9}$$

where $k_{yn} = nG$ and $k_{xm} = -imG$. The reason for the expansion on the right side of the above equation is because both $\chi_b^{(3)}$ (eq 2) and electric field at the pump frequency can be expressed as a polynomial expansion in terms of e^{Gx} and e^{iGy}. This rigorous plane wave expansion largely simplifies the derivation of the induced electric field by this nonlinear polarization. Compared with conventional approach of convolution with Green's function,[31] our Fourier decomposition scenario in eq 9 avoids the complicated numerical integration process by decomposing the inhomogeneous bulk polarization into a sumation of plane waves whose analytical solution is well established.[33]

After some derivation (see Supporting Information), the driven electric field generated by this bulk nonlinear polarization in the quasistatic limit can be summarized as[2,33]

$$\mathbf{E}^{n,m} = \begin{cases} -\dfrac{1}{\varepsilon_0\varepsilon(\omega_3)} \dfrac{\mathbf{k}_s(\mathbf{k}_s \cdot \mathbf{P}^{n,m})}{k_s^2}, & m^2 \neq n^2 \\ -\dfrac{1}{\varepsilon_0\varepsilon(\omega_3)} \mathbf{P}^{n,m}, & m^2 = n^2 \end{cases} \tag{10}$$

in which $\mathbf{k}_s = (k_{xm}, k_{ny})$ and the total driven electric field is obtained by $\mathbf{E}^D = \sum_n \sum_m \mathbf{E}^{n,m} e^{mGx} e^{inGy}$. Then, by matching the driven electric field at two metal interfaces, i.e., E_y^D at $x = w_1$ and $x = -w_2$, the mode coefficients of the excited third-harmonic field can be computed. Figure 2d illustrates the excited near field and corresponding emission pattern of direct THG. The symmetry property for the near field demonstrates a net dipole along x' direction for a_x mode and y' direction for a_y mode.

The emission pattern can be quantitatively analyzed by calculating the total multipole moments (with an overline) of the nanowire dimer by integrating the polarization function (without overline)[34]

$$\bar{p}'_x = \iint P'_x(x', y')\mathrm{d}x'\ \mathrm{d}y'$$
$$\bar{p}'_y = \iint P'_y(x', y')\mathrm{d}x'\ \mathrm{d}y'$$
$$\bar{Q}'_{xx} = \iint 2x' P'_x(x', y')\mathrm{d}x'\ \mathrm{d}y'$$
$$\bar{Q}'_{yy} = \iint 2y' P'_y(x', y')\mathrm{d}x'\ \mathrm{d}y'$$
$$\bar{Q}'_{xy} = \bar{Q}'_{yx} = \iint (x' P'_y(x', y') + y' P'_x(x', y'))\mathrm{d}x'\ \mathrm{d}y' \tag{11}$$

From the mode symmetry, the value of these multipole moments can be easily deduced. For the near field at pump frequency ω_1 and third-harmonic frequency ω_3 shown in Figure 2a,c,d, P'_x (P'_y) is an even function in relation to both x' and y' for a_x (a_y) mode, making $\bar{p}'_x \neq 0$ for a_x, while $\bar{p}'_y \neq 0$ for a_y. In the quasistatic limit, dipole emission dominates and gives a "figure eight" radiation pattern. In contrast, the

https://doi.org/10.1021/acsphotonics.3c00343
ACS Photonics XXXX, XXX, XXX−XXX

$P'_x(x',y')$ and $P'_y(x',y')$ for the second-harmonic field in Figure 2b are odd functions regarding x' and y', respectively, thereby resulting in a zero net dipole moment $\overline{p}_{x',y'}$. From eq 11, the integrand of $\overline{Q}'_{xx,yy}$ is even, which results in nonzero diagonal terms of quadrupole tensor. However, for the off-diagonal terms of the quadrupole tensor, the odd symmetric property makes $\overline{Q}'_{xy,yx}$ vanish. In summary, the near field at ω_1 and ω_3 is characterized by a net dipole moment $\overline{p}_{x',y'}$, while the second-harmonic field is characterized by a diagonal electric quadrupole tensor.

4. THG SPECTRUM AND SIZE DEPENDENCE

In the above section, we obtained the field profile for direct and cascaded THG and proved that both exhibit a dipole radiation pattern. The THG power in the far field can be evaluated by[35]

$$W_{\mathrm{TH}} = \frac{\omega_3}{2}\mathrm{Im}[\alpha]\left(\frac{|E_{3x}(0,0)|^2}{|1-\beta_x\alpha|} + \frac{|E_{3y}(0,0)|^2}{|1-\beta_y\alpha|}\right) \tag{12}$$

where $E_{3x}(0,0)$ and $E_{3y}(0,0)$ are the third-harmonic electric field at the origin in the MIM frame and $\alpha = i\frac{\varepsilon_0 g^2 h^2 \omega_3^2}{8c^2}$. c and ε_0 are the speed of light and permittivity in the free space, respectively. The detailed expression for $\beta_{x,y}$ is provided in the Supporting Information. In addition, a dimensionless quantity is defined to characterize the THG efficiency, written as $\eta_{\mathrm{TH}} = W_{\mathrm{TH}}/W_{\mathrm{inc}}$ with input power $W_{\mathrm{inc}} = \frac{|\mathbf{E}_{\mathrm{inc}}|^2}{2Z_0(D_1+D_2)}$, where Z_0 is the impedance of free space. To confirm the validity of our theoretical framework, we compare our analytical solution of THG efficiency with Comsol numerical simulation and reach an excellent agreement for a subwavelength nanowire dimer (see Supporting Information).

Figure 3 diagrams the dependence of THG on gap size δ and pump frequency ω_1. In varying the gap size δ, the diameters of two nanowires are maintained. For $\theta = 0°$, the electric polarization along the dimer axis, while for $\theta = 45°$ electric field has an angle 45° to the dimer axis. When the electric field polarizes along the dimer axis, only a_x mode can be excited due to the symmetry in Figure 3a,b. In Figure 3c,d, the polarization angle is changed to $\theta = 45°$, which excites both a_x and a_y modes.

In the limit of large δ, the direct THG in Figure 3a,c has two resonances, where one is ω_{sp}, while the other is $\omega_{sp}/3$. ω_{sp} and $\omega_{sp}/3$ correspond to the mode excitation of a single nanowire at pump frequency ω_1 and third-harmonic frequency ω_3, respectively. When shrinking the gap size, δ, more modes stem from these two resonances and distribute into a broader frequency range, as shown in Figure 3a,c. The mode excitation at ω_1 being stronger than that at ω_3 is because the THG by enhancing the pump field is more efficient than that by enhancing the third-harmonic field according to eq 4.

On the contrary, the large-δ limit for cascaded THG in Figure 3b,d has three resonances: ω_{sp}, $\omega_{sp}/2$, and $\omega_{sp}/3$. They correspond to the mode excitation of a nanowire at the pump, second-harmonic, and third-harmonic frequencies, respectively. Like the direct THG, the mode splits and evolves into a broader frequency range when decreasing the gap size δ. The additional mode excitation at ω_2 is one fingerprint that differentiates the cascaded from the direct THG. An

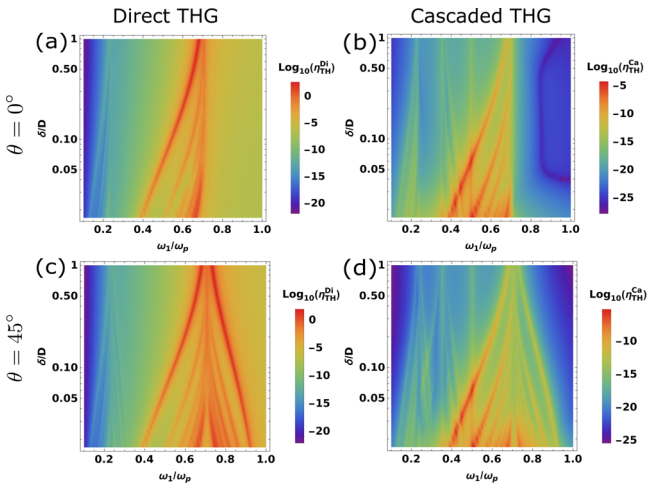

Figure 3. THG efficiency η_{TH} as a function of gap size δ and pump frequency ω_1 with fixed nanowire diameters $D_1 = D_2 = 6$ nm. Mode evolution of the THG spectrum when varying δ is investigated. (a) Direct THG when the pump electric field polarized along the dimer axis; (b) Cascaded THG when the pump electric field polarized along the dimer axis; (c) Direct THG when the angle between electric field direction and dimer axis is $\theta = 45°$; (d) Cascaded THG when the angle between electric field direction and dimer axis is $\theta = 45°$. Note that the axes of δ and THG efficiency η_{TH} are presented in the log scale. The superscripts "Di" and "Ca" represent the direct and cascaded processes, respectively.

interesting effect is that modes originate from ω_{sp}, $\omega_{sp}/2$, and $\omega_{sp}/3$ that overlap with each other to form multiresonant states. It can be observed from the color map in Figure 3 that the multiresonance further enhances the THG efficiency. In the singular limit, i.e., $\delta \to 0$, the THG mode spectrum becomes continuous,[7] leading to a broadband and continuous multiresonant state.

The evolution of modes in Figure 3 can be quantitatively described by the dispersion relation of a nanowire dimer. A nanowire dimer with identical diameters supports a_x and a_y modes with opposite symmetries, as depicted in Figure 2a. By looking at the pole of the coefficients of the excited field, the dispersion relations for these two modes read[8,15]

$$\begin{cases} (\sqrt{\rho} + \sqrt{1+\rho})^{4n} = \mathrm{Re}\left[\dfrac{\varepsilon - 1}{\varepsilon + 1}\right], & a_x \text{ mode} \\ (\sqrt{\rho} + \sqrt{1+\rho})^{4n} = \mathrm{Re}\left[\dfrac{1 - \varepsilon}{\varepsilon + 1}\right], & a_y \text{ mode} \end{cases} \tag{13}$$

where $\rho = \delta/2D$. The direct THG has two sets of eq 13 with $\omega = \omega_1$ and $\omega = \omega_3$, while the cascaded possesses three sets of eq 13 with $\omega = \omega_1$, $\omega = \omega_2$, and $\omega = \omega_3$. A property of eq 13 is that the $a_x(a_y)$ mode resides on the left(right) side of $\omega = \omega_{sp}$. When the pump electric field polarized along the dimer axis, the ω_1 and ω_3 branches of mode for direct THG in Figure 3a correspond to the a_x-type mode dispersion in eq 13. Similarly, the cascaded THG in Figure 3b also exhibits the a_x-type dispersion relation for the ω_1 and ω_3 branches. However, the additional ω_2 branch of cascaded THG shows an a_y-type dispersion relation in Figure 3b. This discrepancy is because that induced surface polarization has a quadradic relation with the pump electric field, changing the field symmetry of the excited second-harmonic mode. When the electric field is not

https://doi.org/10.1021/acsphotonics.3c00343
ACS Photonics XXXX, XXX, XXX−XXX

collinear with the dimer axis, both a_x-type and a_y-type resonance appears and can be described with eq 13.

We further note that the cascaded THG has two dispersionless modes when varying the gap size. From eq 8, $\varepsilon_b \to 0$ contributes to a divergent magnetic current, resulting in a giant harmonic generation at either $\omega = \omega_p/2$ or $\omega = \omega_p/3$.

The plasmonic nanostructure in the quasistatic approximation has interesting size dependence. It has been suggested that the electric field profile for the linear optical response preserves when changing the size of nanostructures (keeping δ/D as a constant).[23,35] However, as far as we know, the size-dependence feature for the nonlinear optical response of nanostructures has not been analyzed yet. Here, we summarize the size-dependence properties for the electric field and power at ω_1, ω_2, and ω_3 in Table 1, where $W_{ext,sca}$ is power extinction

Table 1. Size-Dependence Rule

ω_1	ω_2	ω_3
$E_1' \propto 1$	$E_2' \propto D^{-1}$	$E_3^{Di\prime} \propto 1$
$W_{ext} \propto D^2$	$W_{SH}^{dipole} \propto D^2$	$W_{TH}^{Di} \propto D^4$
$W_{sca} \propto D^4$	$W_{SH}^{quad} \propto D^4$	$E_3^{Ca\prime} \propto D^{-2}$
		$W_{TH}^{Ca} \propto 1$

and scattered in the linear optical response, $W_{SH}^{dipole,quad}$ is the SHG power by the dipole/quadrupole moment. We do not differentiate the power in two frames because the energy is conserved.

Here, we briefly interpret the size-dependence behavior for the nonlinear optical response. For the SHG process in the cascaded THG, the size-independent E_1' induces a size-independent nonlinear surface polarization. However, the derivative of surface polarization in the definition of the magnetic current (eq 8) is inversely proportional to the length scale, making excited second-harmonic field E_2' inversely proportional to D. Then by integrating the polarization with eq 11, the total dipole and quadrupole moment obtain a D and D^2 dependence, respectively. Being proportional to the square of each multipole moment, the dipole emission power $W_{SH}^{dipole} \propto D^2$ and quadrupole emission $W_{SH}^{quad} \propto D^4$. In the SFG process, the induced surface polarization at ω_3 has a D^{-1} dependence, making the $E_3^{Ca'} \propto D^{-2}$ following the similar interpretation of SHG. The total dipole moment due to $E_3^{Ca'}$ is size-independent, leading to a size-independent W_{TH}^{Ca}. For the direct THG, the size-independent E_1' contributes a size-independent nonlinear polarization $\mathbf{P}^{NL\prime}$, exciting a size-independent $E_3^{Di'}$. The $E_3^{Di'}$ induced total dipole menmentum gains a dependence on D^2, making the $W_{TH}^{Di} \propto D^4$.

Figure 4a diagrams the dependence of direct THG power W_{TH}^{Di} on the diameter of nanowire D, which confirms a D^4 dependence of W_{TH}^{Di} in the quasistatic region. When further increasing the size of the nanowire, the W_{TH}^{Di}/D^4 ceases to be a constant due to the retardation effect. Unlike the direct THG, the cascaded THG power W_{TH}^{Ca} is size-independent in the quasistatic region and decreases in the retarded region. As a result of different size dependence, the direct and cascaded THG powers are expected to have a critical point where two powers equal. In Figure 4c, we plot these two power as a function of nanowire diameter D and electron density of plasmonic material, where a clear crossing appears. The cascaded THG dominates in the limit of small D and lower electron density (such as semiconductor). On the contrary, the

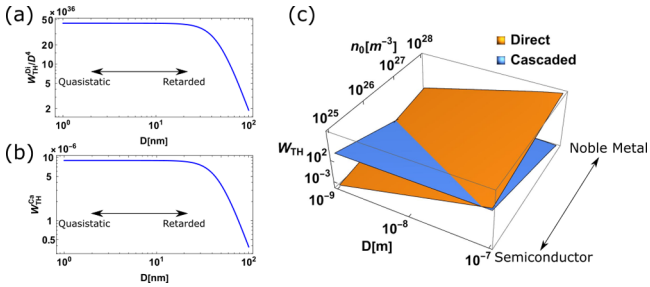

Figure 4. Size-dependence property of THG from a nanowire dimer with fixed ratio $D/\delta = 6$. (a) The dependence of W_{TH}^{Di}/D^4 on the structure size parameter D. In the small-D limit (quasistatic), the flat curve confirms the size independence of W_{TH}^{Di}/D^4; (b) The dependence of W_{TH}^{Ca} on the structure size parameter D. With quasistatic approximation, W_{TH}^{Ca} is independent of D; (c) The THG efficiency in η_{TH} as a function of nanowire diameter $D = D_1 = D_2$ and electron density n_0 for the direct and cascaded processes. The frequency is $\omega_F = 0.58\omega_p$, corresponding to a plasmonic mode shown in Figure 2. By tuning the electron density, the corresponding plasmon frequency $\omega_p = \sqrt{\frac{e^2 n_0}{\varepsilon_0 m_e}}$ is simultaneously modified.

direct THG prevails in the limit of large D and high electron density (such as noble metal). The significance of Figure 4 is that we can experimentally measure the size dependence of THG power to clarify its direct or cascaded origin.

5. CONCLUSION

The THG from nanowire dimer geometry is analytically investigated by using transformation optics. Introducing transformation optics is essential because we can look at the direct and cascaded THG problem in an analytical scenario for complex nanostructures. In addition, we in this paper have found that the direct and cascaded THG have different spectrum and size dependence, which can be used as a fingerprint in future experiments to distinguish the SHG origin of a nanostructure. Furthermore, by making the nanostructure singular, a broadband continuous multiresonant state emerges, substantially enhancing THG efficiency. Moreover, despite a plasmonic nanowire being considered, our theory can be readily applied in a dielectric system whose validity has been numerically verified in the Supporting Information. Besides, for a simple clarification of the idea, this paper does not consider the nonclassical effects, such as nonlocality and electron spill-out. These nonclassical effects play an indispensable role for a dimer with a subnanometer gap, requiring further exploration. Finally, the analytical framework for the direct THG process can be readily extended to the Kerr-type nonlinearity problem, which will be left for a later paper.

■ ASSOCIATED CONTENT

Supporting Information

The Supporting Information is available free of charge at https://pubs.acs.org/doi/10.1021/acsphotonics.3c00343.

The detailed analytical derivation for linear optical response, transformation rule of $\chi_b^{(3)}$ and $\chi_s^{(2)}$, second-order nonlinear surface susceptibility, direct and cascaded THG calculation, and emission power of THG are provided. In addition, the setting for numerical simulation in Comsol and a comparison between the analytical and numerical solutions are also given (PDF)

https://doi.org/10.1021/acsphotonics.3c00343
ACS Photonics XXXX, XXX, XXX−XXX

AUTHOR INFORMATION

Corresponding Author

Fan Yang − *College of Physics, Key Laboratory of High Energy Density Physics and Technology of the Ministry of Education, Sichuan University, Chengdu, Sichuan 610065, China;* orcid.org/0000-0002-8648-1858; Email: fyang@scu.edu.cn

Author

Cristian Ciracì − *Istituto Italiano di Tecnologia, Center for Biomolecular Nanotechnologies, 73010 Arnesano, Italy;* orcid.org/0000-0003-3349-8389

Complete contact information is available at: https://pubs.acs.org/10.1021/acsphotonics.3c00343

Notes

The authors declare no competing financial interest.

ACKNOWLEDGMENTS

F.Y. acknowledges the financial support from the National Natural Science Foundation of China (Grant No. 12204328), the Fundamental Research Funds for the Central Universities, and Science Specialty Program (Grant No. 2020SCUNL210) from Sichuan University. C.C. acknowledges funding from the European Union's Horizon Europe Research and Innovation Program (Grant Agreement No. 101046329).

REFERENCES

(1) Boyd, R. W. *Nonlinear Optics*; Academic Press, 2020.

(2) Shen, Y.-R. *Principles of Nonlinear Optics*; Wiley-Interscience: New York, NY, U.S.A., 1984.

(3) Krasavin, A. V.; Ginzburg, P.; Zayats, A. V. Free-electron optical nonlinearities in plasmonic nanostructures: a review of the hydrodynamic description. *Laser & Photonics Reviews* **2018**, *12*, 1700082.

(4) De Luca, F.; Ortolani, M.; Ciracì, C. Free electron nonlinearities in heavily doped semiconductors plasmonics. *Phys. Rev. B* **2021**, *103*, 115305.

(5) Celebrano, M.; Locatelli, A.; Ghirardini, L.; Pellegrini, G.; Biagioni, P.; Zilli, A.; Wu, X.; Grossmann, S.; Carletti, L.; De Angelis, C.; et al. Evidence of cascaded third-harmonic generation in noncentrosymmetric gold nanoantennas. *Nano Lett.* **2019**, *19*, 7013−7020.

(6) Celebrano, M.; Wu, X.; Baselli, M.; Großmann, S.; Biagioni, P.; Locatelli, A.; De Angelis, C.; Cerullo, G.; Osellame, R.; Hecht, B.; et al. Mode matching in multiresonant plasmonic nanoantennas for enhanced second harmonic generation. *Nat. Nanotechnol.* **2015**, *10*, 412−417.

(7) Pendry, J. B.; Aubry, A.; Smith, D.; Maier, S. A. Transformation optics and subwavelength control of light. *science* **2012**, *337*, 549−552.

(8) Aubry, A.; Lei, D. Y.; Maier, S. A.; Pendry, J. Interaction between plasmonic nanoparticles revisited with transformation optics. *Physical review letters* **2010**, *105*, 233901.

(9) Talley, C. E.; Jackson, J. B.; Oubre, C.; Grady, N. K.; Hollars, C. W.; Lane, S. M.; Huser, T. R.; Nordlander, P.; Halas, N. J. Surface-enhanced Raman scattering from individual Au nanoparticles and nanoparticle dimer substrates. *Nano Lett.* **2005**, *5*, 1569−1574.

(10) Fernández-Domínguez, A. I.; Zhang, P.; Luo, Y.; Maier, S.; García-Vidal, F.; Pendry, J. Transformation-optics insight into nonlocal effects in separated nanowires. *Phys. Rev. B* **2012**, *86*, 241110.

(11) Luo, Y.; Fernandez-Dominguez, A.; Wiener, A.; Maier, S. A.; Pendry, J. Surface plasmons and nonlocality: a simple model. *Physical review letters* **2013**, *111*, 093901.

(12) Savage, K. J.; Hawkeye, M. M.; Esteban, R.; Borisov, A. G.; Aizpurua, J.; Baumberg, J. J. Revealing the quantum regime in tunnelling plasmonics. *Nature* **2012**, *491*, 574−577.

(13) Scholl, J. A.; García-Etxarri, A.; Koh, A. L.; Dionne, J. A. Observation of quantum tunneling between two plasmonic nanoparticles. *Nano Lett.* **2013**, *13*, 564−569.

(14) Zhu, W.; Esteban, R.; Borisov, A. G.; Baumberg, J. J.; Nordlander, P.; Lezec, H. J.; Aizpurua, J.; Crozier, K. B. Quantum mechanical effects in plasmonic structures with subnanometre gaps. *Nat. Commun.* **2016**, *7*, 1−14.

(15) Yang, F.; Ding, K. Transformation optics approach to mesoscopic plasmonics. *Phys. Rev. B* **2022**, *105*, L121410.

(16) Li, R.-Q.; Hernángomez-Pérez, D.; García-Vidal, F.; Fernández-Domínguez, A. Transformation optics approach to plasmon-exciton strong coupling in nanocavities. *Physical review letters* **2016**, *117*, 107401.

(17) Pendry, J.; Fernández-Domínguez, A.; Luo, Y.; Zhao, R. Capturing photons with transformation optics. *Nat. Phys.* **2013**, *9*, 518−522.

(18) Reddy, K. N.; Chen, P. Y.; Fernández-Domínguez, A. I.; Sivan, Y. Surface second-harmonic generation from metallic-nanoparticle configurations: A transformation-optics approach. *Phys. Rev. B* **2019**, *99*, 235429.

(19) Elkabetz, S.; Reddy, K. N.; Chen, P. Y.; Fernández-Domínguez, A. I.; Sivan, Y. Optimization of second-harmonic generation from touching plasmonic wires. *Phys. Rev. B* **2021**, *103*, 075411.

(20) Yang, F.; Ciracì, C. Second-harmonic generation from singular metasurfaces. *Phys. Rev. B* **2022**, *105*, 235432.

(21) Kittel, C.; McEuen, P. *Introduction to Solid State Physics*; John Wiley & Sons, 2018.

(22) Ashcroft, N. W.; Mermin, N. D. *Solid State Physics*; Cengage Learning, 2022.

(23) Aubry, A.; Lei, D. Y.; Fernández-Domínguez, A. I.; Sonnefraud, Y.; Maier, S. A.; Pendry, J. B. Plasmonic light-harvesting devices over the whole visible spectrum. *Nano Lett.* **2010**, *10*, 2574−2579.

(24) Aubry, A.; Lei, D. Y.; Maier, S. A.; Pendry, J. B. Plasmonic hybridization between nanowires and a metallic surface: a transformation optics approach. *ACS Nano* **2011**, *5*, 3293−3308.

(25) Pendry, J.; Huidobro, P. A.; Luo, Y.; Galiffi, E. Compacted dimensions and singular plasmonic surfaces. *Science* **2017**, *358*, 915−917.

(26) Yang, F.; Huidobro, P. A.; Pendry, J. B. Transformation optics approach to singular metasurfaces. *Phys. Rev. B* **2018**, *98*, 125409.

(27) Boyd, R. W.; Shi, Z.; De Leon, I. The third-order nonlinear optical susceptibility of gold. *Opt. Commun.* **2014**, *326*, 74−79.

(28) Ciracì, C.; Poutrina, E.; Scalora, M.; Smith, D. R. Origin of second-harmonic generation enhancement in optical split-ring resonators. *Phys. Rev. B* **2012**, *85*, 201403.

(29) De Luca, F.; Ciracì, C. Difference-frequency generation in plasmonic nanostructures: a parameter-free hydrodynamic description. *JOSA B* **2019**, *36*, 1979−1986.

(30) Maier, S. A. *Plasmonics: Fundamentals and Applications*; Springer, 2007; Vol. *1*.

(31) Reddy, K. N.; Chen, P. Y.; Fernández-Domínguez, A. I.; Sivan, Y. Revisiting the boundary conditions for second-harmonic generation at metal-dielectric interfaces. *J. Opt. Soc. Am. B* **2017**, *34*, 1824−1832.

(32) Albooyeh, M. Electromagnetic Characterization of Metasurfaces. *Ph.D. Thesis*, Aalto University, 2015.

(33) Bloembergen, N.; Pershan, P. Light waves at the boundary of nonlinear media. *Physical review* **1962**, *128*, 606.

(34) Stratton, J. A. *Electromagnetic Theory*; John Wiley & Sons, 2007; Vol. 33.

(35) Aubry, A.; Lei, D. Y.; Maier, S. A.; Pendry, J. Conformal transformation applied to plasmonics beyond the quasistatic limit. *Phys. Rev. B* **2010**, *82*, 205109.